



Insight into the effects of the oxygen species over Ni/ZrO₂ catalyst surface on methane reforming with carbon dioxide

Meng Zhang^{a,b}, Junfeng Zhang^{a,*}, Yingquan Wu^a, Junxuan Pan^a, Qingde Zhang^a, Yisheng Tan^a, Yizhuo Han^{a,*}

^a State Key Laboratory of Coal Conversion, Institute of Coal Chemistry, Chinese Academy of Sciences, Taiyuan, 030001, China

^b University of Chinese Academy of Sciences, Beijing, 100049, China



ARTICLE INFO

Keywords:

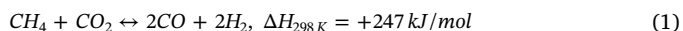
Dry reforming
Ni/ZrO₂ catalysts
Oxygen species
Carbon dioxide
Methane

ABSTRACT

Carbon deposition on the catalyst surface has been considered as one of the main reasons to cause Ni catalyst deactivation during methane reforming with carbon dioxide (DRM). Generally, it is thought that the properties and levels of coke formation are significantly affected by the ability of CO₂ adsorption and activation, which is closely related to the oxygen species over catalyst surface. In this study, the effects of oxygen species on the DRM over Ni/ZrO₂ catalysts were investigated. Wherein, ZrO₂ support was further treated under H₂, N₂, and O₂ atmospheres respectively to obtain different oxygen species distribution over the surface, and 3 wt.% Ni was introduced by the deposition-precipitation method. The representative samples were characterized using XRD, EPR, XPS, FTIR, TPR, TPD, TPSR, TG, Raman and TPH techniques, etc. It was found that the treatment to ZrO₂ in the reducing gas such as H₂ was able to promote the formation of adsorbed oxygen species over the surface. CO₂ DRIFTS and CH₄-TPSR experiments further confirmed that adsorbed oxygen species were favorable for enhancing both CO₂ adsorption and activation and CH₄ dissociation. As a result, the catalyst with more adsorbed oxygen species exhibited relatively outstanding performance for the DRM and promotional ability in removal of the deposited carbon.

1. Introduction

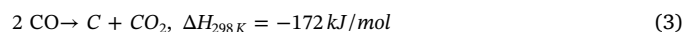
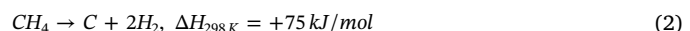
Global warming has been expected to be one of the most difficult scientific challenges at present. Methane reforming with carbon dioxide (Eq. (1)), known as dry reforming of methane (DRM), has attracted growing attentions recently because of the simultaneous utilization of two greenhouse gases, CH₄ and CO₂ [1]. In addition, the synthesis gas (H₂ + CO) produced has lower and uniform H₂/CO ratio than that generated from steam reforming and partial oxidation of methane. The low H₂/CO ratio synthesis gas is favorable for the synthesis of highly valuable oxygenated chemicals and long-chain hydrocarbons [2,3].



Ni catalyst, because of the comparable activity and stability to noble metal catalysts, has been considered as the most promising catalyst for the DRM [1,4] as well as steam reforming [5], partial oxidation of methane [6] and tri-reforming [7]. Despite that lots of work has been done in the past couple of decades, the present main issue is that the Ni catalyst employed shows a rapid deactivation induced by the carbon deposition and sintering of Ni particles under the rigorous reaction

conditions. By now, the Ni catalyst has still kept absent in the industrial application [8,9].

In the DRM, carbon deposition is mainly caused by CH₄ decomposition and CO disproportionation (Eqs. (2) and (3), respectively). Wherein, thermally, the former (1) is favored at high temperature and low pressure, while the latter is easily promoted at low temperature and high pressure. Generally, the DRM is performed at the atmospheric pressure and above 700 °C, thus, deposited carbon on the catalyst surface is mainly originated from CH₄ decomposition [10].



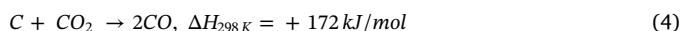
Previous reports have well demonstrated that small-size Ni particles are relatively effective to suppress the carbon deposition in the DRM [11–13]. Two strategies have been adopted to improve the carbon-resistant ability of Ni catalyst. One is to obtain the catalysts with smaller nickel particle or higher nickel dispersion by controlling and modifying the preparation method [14,15]. The other is to encapsulate Ni particles mainly using SiO₂, Al₂O₃, TiO₂, ZrO₂, etc. [16–18] (so-called

* Corresponding authors at: Institute of Coal Chemistry, Chinese Academy of Sciences, Taiyuan, 030001, China.

E-mail addresses: zhangjf@sxicc.ac.cn (J. Zhang), hanyz@sxicc.ac.cn (Y. Han).

confinement effect) to avoid the aggregation of nickel particles.

Factually, during the DRM, adsorption and activation of CO₂ are of equal importance to eliminate the deposited carbon (Eq. (4)). Therefore, on account of the dual function nature of Ni catalyst for the DRM [19–21], improving the ability of adsorption and activation CO₂ should be paid more attention as well. It has been demonstrated that both strong basicity and oxygen mobility can promote the chemisorption of CO₂ and implement the removal of deposited carbon [22,23]. Herein, ZrO₂, with quite high thermal stability and surface oxygen mobility, which possesses four chemical properties on the surface, acidic and basic properties and oxidizing and reducing properties [24], has been applied in the DRM as promoter [25] or support [26,27].



So far, a series of considerable progress has been made in this regard, however, most of the previous researches principally focused on the correlation of catalyst activity with its physicochemical properties [26,28,29]. In previous work, our group has proved that the crystalline structure of ZrO₂ support plays an important role in enhancing the performance of the catalyst for the DRM, especially promoting the stability and coke-resistant ability [30]. Also, we have illustrated that the morphology of ZrO₂ has significant influences on the DRM [31]. Nevertheless, there is still no enough illustration for the relationship between the adsorption and activation of CO₂ and the oxygen species over the catalyst surface in the DRM, as well as the consideration on the suppression and removal of the deposited carbon.

Therefore, we, in this work, have systematically studied the influence of the oxygen species over ZrO₂ supports surface on CO₂ adsorption and activation as well as catalytic performance in the DRM over Ni/ZrO₂ catalysts. Wherein, the oxygen species of the ZrO₂ support were tuned by treatment under different atmospheres, such as H₂, O₂ and N₂. Based on the characterization results, CO₂ DRIFTS and CH₄-TPSR experiments, it was found that the catalyst with more adsorbed oxygen species, which was treated under H₂ atmosphere, showed relatively good performance in the DRM and the ability of carbon removal, due to enhancing the adsorption and activation of CO₂.

2. Experimental

2.1. Catalyst preparation

Zirconium dioxide (ZrO₂, purity 99.99%, Aladdin Industrial Corporation), nickel (II) nitrate hexahydrate [Ni(NO₃)₂·6H₂O, purity 98.0%, Sinopharm Chemical Reagent Co. Ltd], sodium carbonate anhydrous (Na₂CO₃, purity 99.8%, Tianjin Feng Chuan Chemical Reagent Co. Ltd) were used in the experiments without further purification.

As reported, the preparation method [32], calcination temperature [33] and atmospheres [34] during synthesis may significantly affect the crystalline structure and textural properties of support and catalyst. Therefore, it is necessary to pre-stabilize the above-mentioned properties to deeply investigate the effect of single factor on the catalytic performance in the DRM.

In present work, the purchased ZrO₂ sample was treated with a rise of heating ramp of 2 °C/min in the muffle furnace at 800 °C for 4 h firstly and the sample was simplified as ZR. Afterward, ZR sample was divided into three parts, and every part was calcined at 750 °C in the tube furnace under the flow H₂, N₂, and O₂ atmosphere (30 mL/min) with the heating ramp of 2 °C/min, respectively. The three resulting samples were referred to ZRH, ZRN and ZRO.

In order to minimize the influences of the chemical state of Ni particles, the Ni loading of Ni/ZrO₂ catalysts was chosen as low as 3 wt. %, and the catalysts were prepared using deposition-precipitation method. Typically, a stoichiometric aqueous solution containing Ni (NO₃)₂ (0.05 M) was heated to 60 °C, accompanied by the rigorous stirring. Then, ZrO₂ samples treated with different atmospheres were put into the solution. After that, the aqueous solution of Na₂CO₃ was

added dropwise to adjust the pH to around 10. The resulting suspension was heated at 60 °C for 4 h with the continuous stirring, followed by being centrifuged and washed several times with distilled water. Finally, the collected samples were dried at 110 °C for 12 h and calcined at 500 °C for 4 h. The obtained catalysts were identified as 3NZx, where x indicates the calcination ambience. For example, 3NZN referred to the catalyst with 3% Ni loading, and the ZrO₂ support treated with the N₂ atmosphere.

2.2. Catalyst characterization

X-ray diffraction (XRD) patterns of the samples were carried out on an X-ray diffractometer (Rigaku, Ultima IV X-ray diffractometer) using Cu K α radiation ($\lambda = 0.15418 \text{ nm}$). The measurement was operated at 40 kV and 40 mA with a scanning rate of 4°/min in the 2θ range of 20–80 °.

The BET surface area and total pore volume of the samples were measured at -196 °C with a nitrogen sorption technique (Micromeritics ASAP 2020). Prior to measurement, the samples were pretreated at 200 °C for 3 h. The specific surface area was calculated via the BET model and the pore size distribution was estimated by the Brunauer-Emmet-Teller (BJH) model using the desorption branch.

Morphology of the sample was measured by a JEOL JEM-2100 transmission electron microscope (TEM) operated at 200 keV. The sample powder was dispersed in ethanol by ultrasonic for 20 min. Then, the suspension was dropped onto a carbon coated copper TEM grid (200 mesh) and dried in air before measurement.

Electron paramagnetic resonance (EPR) spectroscopy was obtained at room temperature on a Bruker EMXPLUS10/12 spectrometer. 20 mg sample was filled in the capillary tube for each measurement. The detailed operation parameters were as below: the center field was 3200.00 G, the microwave frequency was 9.68 GHz, the modulation frequency was 100.00 kHz, the power was 2 mW and the conversion time was 10 ms.

The XPS spectra were recorded using an AXIS ULTRA DLD X-ray photoelectron spectrometer, equipped with a multichannel detector. Charge referencing was done against adventitious carbon (C1 s, 284.8 eV). The Shirley-type background was subtracted from the signals and the recorded spectra was fitted with Gauss-Lorentz curves to determine the surface composition of different samples.

Fourier transform infrared (FT-IR) spectroscopy was conducted on a Bruker Tensor 27 equipped with a diffuse reflectance chamber and a liquid nitrogen detector. An environmental DRIFTS chamber equipped with KBr windows, allowing *in-situ* treatments up to 400 °C under atmospheric pressure (the desired gas flow volume), was coupled to the spectrometer. The spectrum of pure sample was obtained in the range of 600–4 000 cm⁻¹ with a resolution of 64 scans and 4 cm⁻¹ each. Prior to analysis, the ZrO₂ sample was *in-situ* pretreated at 400 °C in a pure Ar flow (30 mL/min) for 60 min.

H₂ temperature programmed reduction (H₂-TPR) and temperature programmed desorption (H₂-TPD) tests were carried out on a Quantachrome Chemstar TPx chemisorption analyzer. 100 mg of sample (20–40 meshes) was firstly pretreated at 300 °C for 60 min under flowing Ar (30 mL/min). TPR measurement was performed through heating the sample to 800 °C from 100 °C at a rate of 5 °C/min with 10% H₂/Ar (v/v, 30 mL/min). The sample via TPR was directly used for TPD measurement, wherein, the sample was heated to 550 °C from room temperature at the ramp heat rate of 5 °C/min. The dispersion of nickel was calculated as: 2 × (area of TPD)/(area of TPR). The Ni particle size was derived from: 1/Ni_{dispersion}.

CO₂ temperature programmed desorption (CO₂-TPD) were examined on a self-made reactor equipped with a TCD detector. The sample filling amount and pretreatment were similar with H₂-TPR. When the reactor cooled down to 50 °C, the sample was exposed on CO₂ (30 mL/min) flow for 20 min. Then, pure Ar (30 mL/min) was introduced until the baseline of the TCD was stable. After that, the reactor

was heated at a rate of 10 °C/min from 50 to 550 °C and the CO₂ desorption signals were monitored by the TCD detector.

CH₄ temperature-programmed surface reactions (CH₄-TPSR) were performed in the same reactor with CO₂-TPD equipped with an on-line mass spectroscopy (Pfeiffer OmniStar). 100 mg (20–40 meshes) catalyst diluted with 300 mg quartz sand (20–40 meshes) was initially reduced by 10% H₂/Ar (v/v, 30 mL/min) flow at 700 °C for 60 min. After cooling down to 100 °C, the reactant gas of 20% CH₄/Ar (v/v, 30 mL/min) was introduced, followed by the increase of temperature from 100 to 900 °C at a heating rate of 5 °C/min. Simultaneously, the m/e intensities at 2 (H₂), 16 (CH₄), 28 (CO) and 44 (CO₂) in the effluent were recorded by the online mass spectrometer.

H₂ temperature-programmed hydrogenation (H₂-TPH) experiments were conducted in the same reactor with CH₄-TPSR. The filling amount of sample and the pretreatment conditions were same as the CO₂-TPD measurement. The m/e intensity at 16 (CH₄) in the effluent was recorded by the online mass spectrometer.

Thermogravimetric analysis (TG) was used to detect the weight loss of the spent catalysts by temperature rising. Trend data was obtained by Rigaku TG-8120 thermogravimetric analyzer. The sample (10 mg) was heated from room temperature to 850 °C at a rate of 10 °C/min under air atmosphere. DTG was the 1st-derivative of thermogravimetric chart. The integral area and peak position of DTG were correlated with the amount and type of carbonaceous species, respectively.

Raman spectroscopy was used to characterize the nature of deposited carbon after reaction. The spectrum was recorded at room temperature using a Horiba LabRam HR-UV800/Jobin-Yvon spectrometer, equipped with He-Ne laser ($\lambda = 632.8$ nm) of 10 mW power and the tested range of wavenumber was 1 200–1 800 cm⁻¹.

2.3. Catalyst evaluation

The DRM reaction was carried out in a fixed-bed quartz micro-reactor with internal diameter of 8 mm. The reaction was conducted at 700 °C under the atmospheric pressure. Typically, 0.4 g catalyst (20–40 meshes) diluted with 1.2 g quartz sand (20–40 meshes) was placed into the reactor. Prior to each test, the catalyst was heated from room temperature to 700 °C at 100 min in a 10% H₂/Ar (v/v, 30 mL/min) atmosphere, and held at 700 °C for 60 min to activate the catalyst. After that, the mixed gas of methane and carbon dioxide at a volume ratio of 1:1 was introduced into the reactor with a gas hourly space velocity (GHSV) of 24,000 mL/(g h). The effluent gases were analyzed online with a gas chromatograph fitted with a packed column (TDX-01) and a thermal conductivity detector (TCD). To remove trace water in the product gases, a cold trap was placed before the detection.

The conversions of CH₄ and CO₂, which were identified as X(CH₄) and X(CO₂), respectively, were calculated as follows (Eqs. (5) and (6)):

$$X(CH_4) = [(F_{in,CH_4} - F_{out,CH_4}) / F_{in,CH_4}] \times 100\% \quad (5)$$

$$X(CO_2) = [(F_{in,CO_2} - F_{out,CO_2}) / F_{in,CO_2}] \times 100\% \quad (6)$$

The selectivity of H₂ and H₂/CO ratio were calculated using following Eqs. (7) and (8):

$$H_2 \text{ selectivity (\%)} = F_{out,H_2} / (2 \times F_{in,CH_4}) \times 100\% \quad (7)$$

$$H_2/CO = F_{out,H_2} / F_{out,CO} \quad (8)$$

where F_{in, i} was the flow rate of each component in the inlet feed, and F_{out, i} was the flow rate of each component in the outlet feed.

3. Results and discussion

3.1. Characterization of un-supported ZrO₂ samples

Fig. S1 shows the XRD patterns of ZrO₂ samples. As observed, the

Table 1

Physicochemical properties of the ZrO₂ samples after treated at 800 °C and further calcined under different atmospheres (H₂, N₂ and O₂) at 750 °C.

Sample	Crystal structure	Crystalline Size ^a (Å)	Specific surface area (m ² /g)	Pore volume (cm ³ /g)	Average pore diameter (nm)
ZR	monoclinic	384 (15)	13.17	0.026	37.77
ZRH	monoclinic	397 (15)	11.93	0.024	45.12
ZRN	monoclinic	380 (16)	11.30	0.024	46.89
ZRO	monoclinic	402 (19)	12.09	0.025	43.77

^a Calculated by Scherrer equation according to the XRD results.

diffraction peaks of all samples are well attributed to the monoclinic ZrO₂ (JCPDS #37-1484). This suggests that the treatment in different atmospheres does not induce the change of crystalline structure of ZrO₂, that is, the thermal treatment at 800 °C is able to stabilize the structure of ZrO₂. From Table 1 and Fig. S2, one can observe that the crystalline size and textural properties of the treated ZrO₂ are nearly similar with one another, consistent with the results of TEM measurement (Fig. S3). This further demonstrates that the treatment atmospheres hardly affect the structure of ZR.

EPR spectroscopy of the ZrO₂ samples are present in Fig. 1a. Based on the spectrum, it is plausible that Zr³⁺ and F-center, which is assigned to the surface defect [33,35], are distributed over the surface of three samples. Furthermore, the intensity of F-center and Zr³⁺ signals increases in the order: ZRO < ZRN < ZRH, indicating that ZRH sample possesses the most defects and highest reducibility.

Fig. 1b shows the CO₂ desorption behavior of the ZrO₂ samples. The profiles all exhibit two CO₂ desorption peaks, ascribed to the weak and strong basic sites. As observed, the areas of the peak at low temperature (~125 °C) are approximate for the three ZrO₂ samples, and nevertheless ones of peak at high temperature are different from each other. The ZRH sample shows relatively big desorption area and higher desorption temperature than other two, implying that more basic sites and stronger basicity exist over the ZRH sample surface.

XPS measurements were carried out to investigate the surface chemical state and the assignment of oxygen species of ZRH, ZRN and ZRO samples. In Fig. 2a, all ZrO₂ samples exhibit photoemission spectra of peaks at around 182 eV and 184 eV ascribed to 3d_{5/2} and 3d_{3/2} electrons of Zr⁴⁺, respectively. The binding energies of Zr 3d_{5/2} for all ZrO₂ samples are lower than the typical binding energy of Zr 3d_{5/2} identified as 182.2 eV [36]. This indicates that Zr⁴⁺ on the surface has been partly reduced to Zr³⁺, consistent with the EPR results. As reported in the literature [37], the transition from Zr⁴⁺ to Zr³⁺ is closely related with CH₄ dissociation. The deviated extent relative to the typical binding energy reveals that the reducibility of the samples is different with each other. Apparently, the binding energy for ZRH sample shifts to lower position (181.63 eV) compared with that for the ZRN sample (181.68 eV) and ZRO sample (181.78 eV), implying that CH₄ dissociation can be probably enhanced for ZRH [37]. In addition, the binding energy of Zr 3d_{5/2} for ZRO sample shifts to the highest position among the three chosen samples, illustrating that the strongest interaction between the surface Zr and O is present on ZRO sample.

The chemical state of oxygen species over the ZrO₂ samples surface is shown in Fig. 2b by fitting the XPS curves, and the relative proportion of surface adsorbed oxygen species (O_{II}) and lattice oxygen species (O_I) is calculated on basis of the XPS data as shown in Table 2. As observed in Fig. 2b, the lower binding energy peak at 529.5 eV is attributed to the surface lattice oxygen species, while the higher binding energy one at 531.5 eV is attributed to the surface adsorbed oxygen species, related to the groups: –OH in water and C – O in CO₃²⁻ [38]. Wherein, CO₃²⁻ is derived from carbonate species trapped by oxygen vacancies [39]. From Table 2, it is noted that the peak area of the adsorbed oxygen species or O_{II}/O_I ratio is the highest for the ZRH sample, suggesting the most oxygen vacancies, followed by the ZRN sample, and lowest for the ZRO

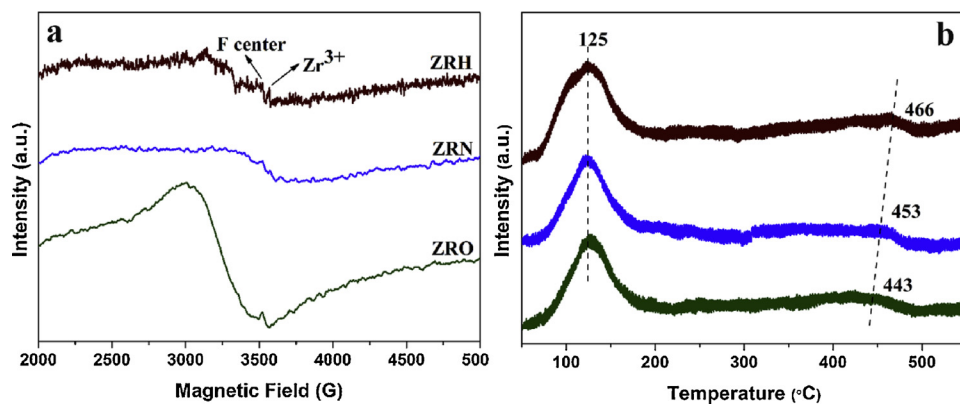


Fig. 1. EPR spectra (a) and CO₂-TPD (b) profiles of the ZrO₂ samples treated under different atmospheres (H₂, N₂ and O₂).

sample. Previous literatures have revealed that the oxygen vacancies have a positive effect on the activation of CO₂ [38,40], which is favorable to suppress carbon deposition. Therefore, the above XPS results imply that our present treated ZrO₂ has an increasing sequence (ZRO < ZRN < ZRH) in the ability of CO₂ activation. Besides, the peaks of the lattice oxygen in the ZRO sample are the highest compared to the other two samples, which means that the oxygen atoms in this sample have interact with Zr atoms more strongly. Conclusively, it is thought that ZrO₂, treated with the reduction atmosphere (via H₂), possesses relatively high reducibility and many oxygen vacancies, which has been considered to exhibit more excellent ability of CH₄ dissociation and CO₂ activation.

To further investigate the CO₂ adsorption on ZrO₂ surface, *in-situ* CO₂ DRIFTS experiments were carried out. Fig. 3 displays the FTIR spectra of the ZrO₂ samples exposed on CO₂ at 400 °C. In Fig. 3a, the bands at 2 358, 2 339 and 2 310 cm⁻¹ are ascribed to the linearly or physically adsorbed CO₂ [41,42]. The intensities of the bands observed for ZRH sample are stronger than that for ZRN and ZRO samples, which indicates that much more linearly or physically adsorbed CO₂ molecules are present on the ZRH sample surface than that on the ZRN and ZRO sample surface.

Furthermore, the adsorption and activation of CO₂ can be also indicated by the carbonate and bicarbonate species formation (Possible (bi-)carbonate species structures on ZrO₂ surface are shown in Tab. S1.). Fig. 3b shows the FTIR spectra in the range of 1 200–1 700 cm⁻¹. The three samples all exhibit bands assigned to carbonate and bicarbonate species. The bands at around 1 397 and 1 670 cm⁻¹ are attributed to ν_s(CO₃) and ν_{as}(CO₃) vibration modes of monodentate bicarbonate species [41,43]. The bands at around 1 418 and 1 620 cm⁻¹ are the characters of bidentate bicarbonate species, attributed to the ν_s(CO₃) and ν_{as}(CO₃) vibration mode, respectively [41,43]. The

Table 2

XPS fitting results of ZrO₂ samples after treated under different atmospheres (H₂, N₂ and O₂).

Sample	BE of Zr 3d _{5/2} (eV)	BE of Zr 3d _{3/2} (eV)	Lattice oxygen (O _I)		Adsorbed oxygen (O _{II})		O _{II} /O _I
			BE (eV)	Area (%)	BE (eV)	Area (%)	
ZRH	181.63	184.03	529.52	58.57	531.48	41.43	0.71
ZRN	181.68	184.18	529.71	60.25	531.54	39.75	0.66
ZRO	181.78	184.23	529.72	63.61	531.45	36.39	0.57

vibration at around 1220 cm⁻¹ is associated with δ(OH) of monodentate/bidentate bicarbonate species [41,43]. The vibrations at the position of α, β, γ, θ and ρ are typical of carbonate complexes. The pair peaks at α and ρ are assigned to the bridged carbonate species, while the pair peaks at β and θ are associated with the bidentate carbonate species [43]. The intensities of the above bicarbonate and carbonate species represent the ability of CO₂ adsorption and activation. For the bands at the position of γ, it has been demonstrated that the stretching of polydentate carbonate species is apparently reasonable [31,44], which represents the acidity of ZrO₂ samples. It is observed that the intensities of these bands for the ZRH samples are higher than that for the ZRN and ZRO samples, except the bands at the position of γ. Conclusively, the above IR results give us that ZRH sample displays the strongest bands for the bridged and bidentate carbonate and bicarbonate species and the weakest bands for the spectra of polydentate carbonate species, suggesting the strongest ability of CO₂ adsorption and activation and the weakest acidity. Thus, the higher ratio of adsorbed oxygen on the sample surface can prompt the CO₂ activation and suppress the acidity.

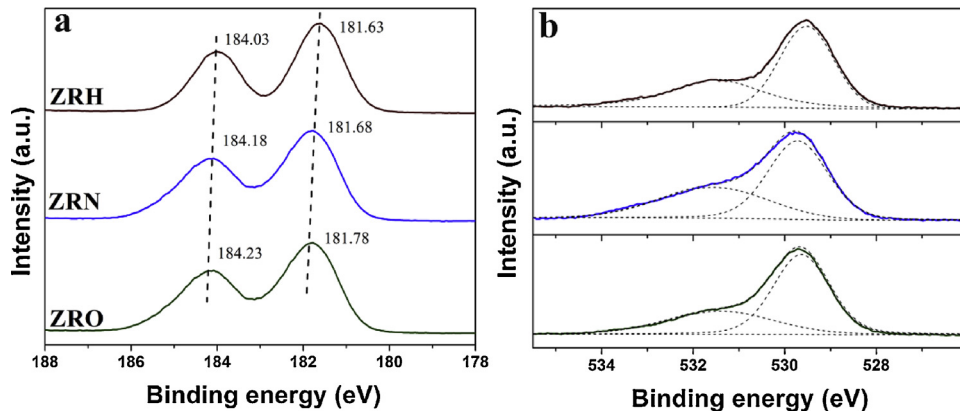
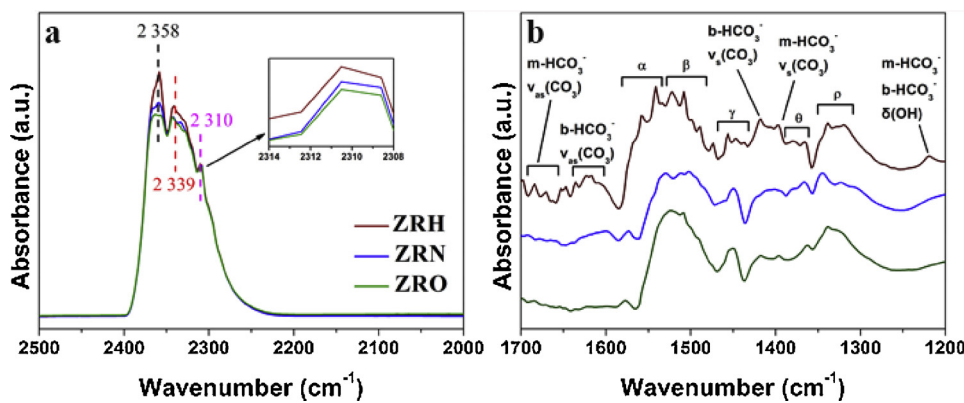


Fig. 2. Zr 3d (a) and O 1 s (b) XPS spectra of the ZrO₂ samples treated under different atmospheres (H₂, N₂ and O₂).



In a word, the structure and textural properties of ZrO_2 are uniform after the high-temperature treatment. While the calcination with different atmospheres is able to obtain different oxygen species distribution over ZrO_2 surface. Further, the oxygen species have been identified to have significant influences on the surface acidity and basicity, especially the ability of CO_2 adsorption and activation. Specifically, the larger amounts of adsorbed oxygen species can promote the adsorption and activation of CO_2 .

3.2. Characterization of ZrO_2 -supported Ni catalysts

The textural properties of ZrO_2 -supported Ni catalysts are shown in Fig. 4 and Table 3. The calculation (from Fig. 4a and b) using the Scherrer equation reveals that the NiO and Ni crystalline sizes are all around 17 and 28 nm, respectively (as listed in Table 3). The results suggest that the high-temperature reduction to the fresh catalysts easily induces the size growth of the dispersed Ni.

The TEM images of the three fresh and reduced catalysts are displayed in Fig. S4 and Fig. 5, respectively. Compared to the corresponding results of unsupported ZrO_2 samples (Fig. S3), there exists no distinct difference in the morphology after the deposition of Ni. Furthermore, it can be observed that the morphology of the fresh catalysts with the ZrO_2 supports treated under different calcination atmospheres do not show obvious difference with each other (Fig. S4). The pore volume slightly increases after Ni loading (compared Table 3 with Table 1), which is probably caused by the agglomerative nickel particles accumulation on the ZrO_2 surface (Fig. S4). Ni particle size was evaluated from Fig. 5 (listed in Table 3). It is obvious that the Ni particles dispersed on three ZrO_2 supports are similar.

H_2 -TPR and H_2 -TPD profiles of the Ni/ ZrO_2 catalysts are displayed in Fig. S5. From Fig. S5a, only one major reduction peak at around 400 °C is observed for the ZrO_2 -supported catalyst. The peak is attributed to the reduction of bulk NiO species, which have weak interaction with the support. Slight shift of the reduction peaks confirmed that NiO

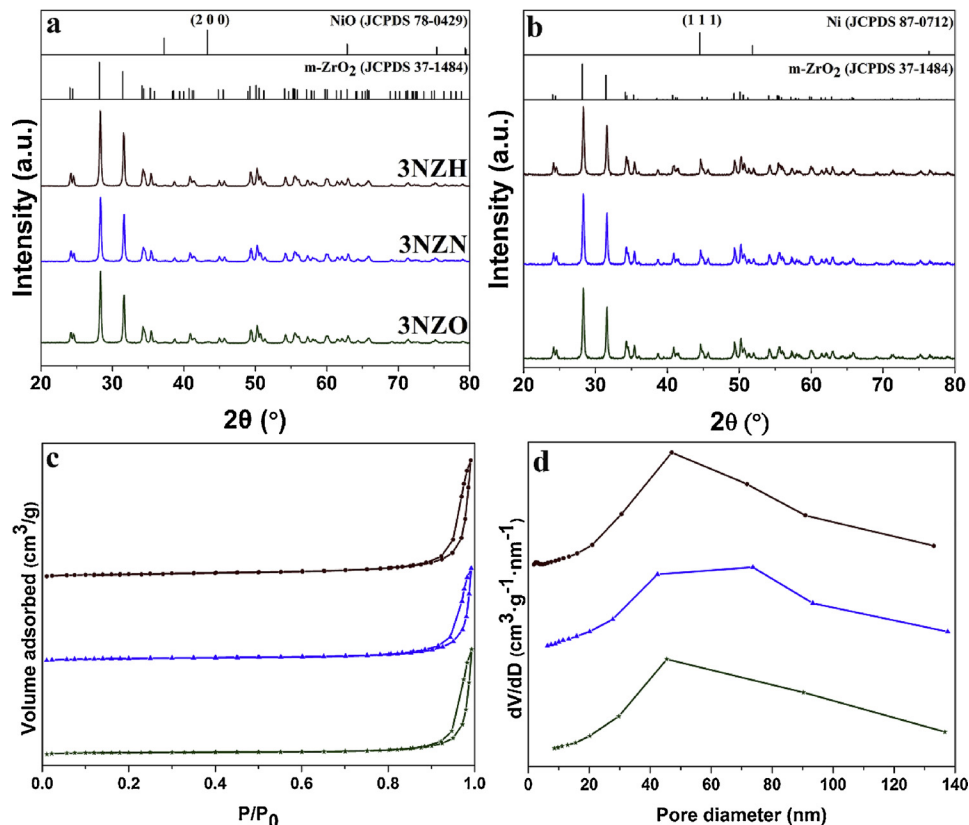


Fig. 4. XRD patterns: fresh (a), reduced (b); N_2 adsorption – desorption isotherms (c) and the pore-size distributions (d) of the Ni-containing catalysts supported by ZrO_2 samples treated under different atmospheres (H_2 , N_2 and O_2).

Table 3

Physicochemical properties of the Ni catalysts supported by the ZrO_2 samples treated under different atmospheres (H_2 , N_2 and O_2).

Sample	Crystalline size (nm)		Specific surface area (m^2/g)	Pore volume (cm^3/g)	Average pore diameter (nm)	Ni dispersion (%)		
	NiO	Ni						
3NZH	16.7	27.2 ^a	12.8 ^b	12.6 ^c	14.02	0.042	36.81	7.8
3NZN	16.2	27.9 ^a	10.5 ^b	11.6 ^c	11.95	0.033	41.87	9.5
3NZO	17.1	28.4 ^a	11.6 ^b	12.3 ^c	10.25	0.034	46.13	8.6

^{a,b} and ^c: Obtained by XRD, Ni dispersion and TEM results, respectively.

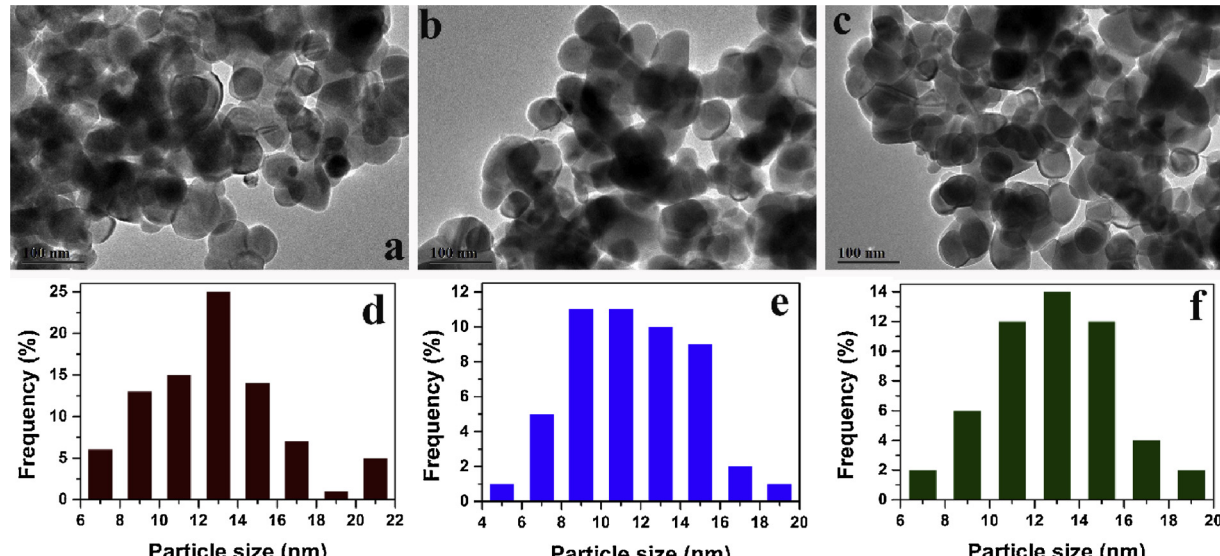


Fig. 5. TEM images: 3NZH (a), 3NZN (b) and 3NZO (c); Ni particle size distributions: 3NZH (d), 3NZN (e), 3NZO (f) of the Ni-containing catalysts supported by ZrO_2 samples treated under different atmospheres (H_2 , N_2 and O_2).

particle is nearly dispersed on the three supports. From the H_2 -TPD profiles (Fig. S5b), the H_2 desorption behavior on the three catalysts is slightly different. Further calculation reveals that Ni dispersion is 7.8, 9.5 and 8.6% for 3NZH, 3NZN and 3NZO catalyst, respectively (as listed in Table 3), and the size of Ni particles on 3NZH, 3NZN and 3NZO catalysts is approximate to each other (listed in Table 3), consisting with the TEM results. This implies slight effect of the size on the catalytic performance in the DRM.

Fig. 6a shows the results of the Ni $2\text{p}_{3/2}$ XPS spectra of the reduced catalysts. All catalysts exhibit three peaks at 861.3 eV, 855.5 eV and 852.4 eV. The peak at 852.4 eV is attributed to metallic Ni component and the peak at 855.5 eV with the satellite peaks at 861.3 eV is assigned to Ni^{2+} , which is resulted from the Ni particles re-oxidized due to the

contact with air after reduction. It has been reported the typical binding energy of Ni $2\text{p}_{3/2}$ for pure NiO is about 854.4 eV [36]. Therefore, it can be deduced that the deviation of the present catalysts with the typical value is mainly related to the interaction between metallic Ni and the support, also identified by the H_2 -TPR profiles.

In addition, it is also noted that the distribution of oxygen species (shown in Fig. 6b and Tab. S2) over the Ni-containing catalysts surface has the same sequence with the supports. This further demonstrates that the Ni loading as low as 3 wt% affects ZrO_2 hardly. However, also it is noteworthy that the ratio of adsorbed oxygen species is lower than the results displayed in Fig. 2b and Table 2. It is thought that the decrease of adsorbed oxygen species is probably caused by the coverage of Ni.

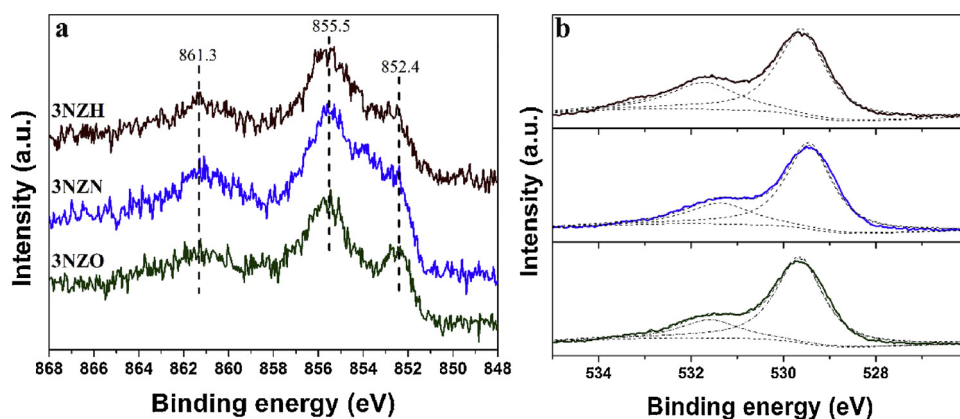


Fig. 6. Ni $2\text{p}_{3/2}$ (a) and O 1s XPS spectra of the reduced Ni-containing catalysts supported by ZrO_2 samples treated under different atmospheres (H_2 , N_2 and O_2).

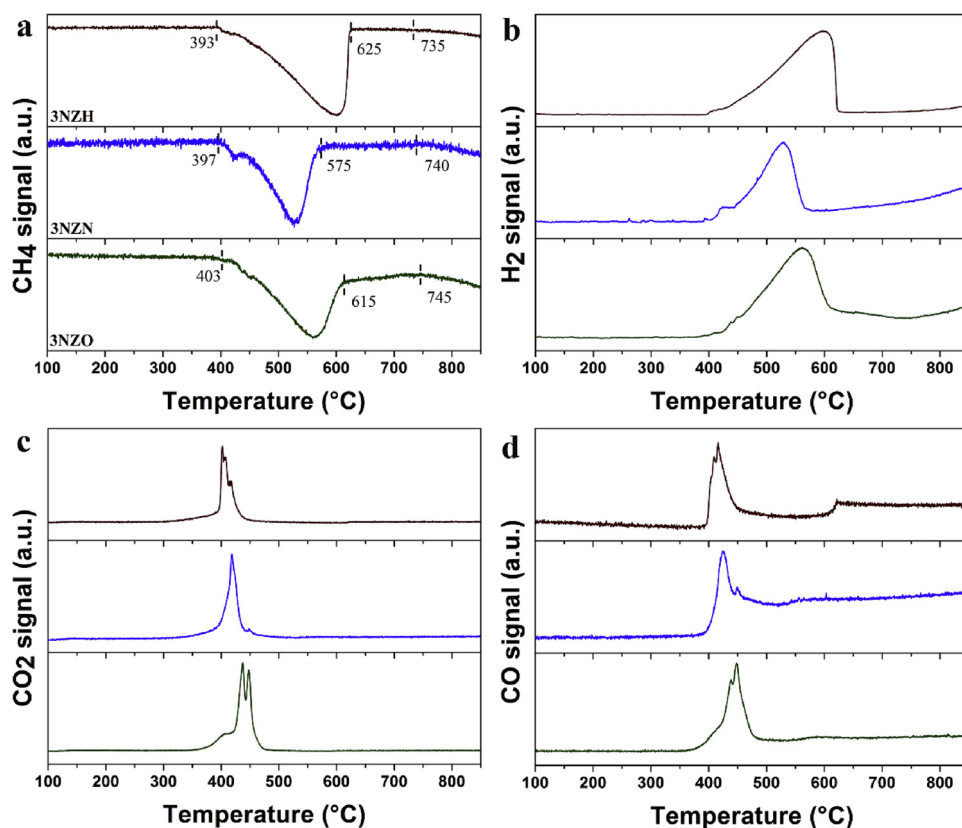


Fig. 7. CH₄-TPSR profiles: (a) CH₄ signal; (b) H₂ signal; (c) CO₂ signal; (d) CO signal over the reduced Ni-containing catalysts supported by ZrO₂ samples treated under different atmospheres (H₂, N₂ and O₂).

In the absence of CO₂, the reactivity of CH₄ dissociation over the three catalysts was investigated by performing CH₄ temperature programmed surface reaction (CH₄-TPSR). Mass signals of CH₄, H₂, CO and CO₂ in the system are recorded, and the results are given in Fig. 7. From Fig. 7a and b, the initial temperatures for CH₄ dissociation and H₂ formation are following in the order of 3NZH (393 °C) < 3NZN (397 °C) < 3NZO (403 °C). Many literatures [13,45,46] have revealed that Ni particle size and the interaction with the support have obviously promotional influence on CH₄ dissociation. Our above result based on the Ni dispersion has demonstrated that 3NZH has slightly larger Ni particle size than other two, whereas the initial temperatures for the present CH₄ dissociation is the lowest on the 3NZH. Considering the similar interaction between Ni and ZrO₂ on the present three catalysts, it is reasonably thought that the present TPSR result is not dependable on the Ni particle size (that is, Ni dispersion) and oxygen species over the catalysts surface probably act as a fairly important role to affect the catalytic activity certainly. In combination with the XPS results, it is apparent that the adsorbed oxygen species have the potential to accelerate CH₄ dissociation.

In TPSR, the carbon stemmed from CH₄ dissociation covers the nickel active sites, thereby leading to the catalyst deactivation. For the 3NZH catalyst, the widest temperature window (393–625 °C) is observed during CH₄ dissociation and H₂ evolution. In case of 3NZN catalyst, a narrowest temperature range (397–575 °C) is observed, whereas, 3NZO catalyst shows an increased temperature region (403–615 °C). The above results indicate that 3NZH catalyst have the best anti-coking ability. Therefore, it is plausible that the adsorbed oxygen species over the surface have positive effects on improving the ability of carbon resistance. Yet, the relatively wide temperature region of 3NZO catalyst than 3NZN catalyst is ascribed to the former poor activity of CH₄ dissociation.

Fig. 7c and d show the recorded signal profiles of CO₂ and CO during CH₄-TPSR. The main evolution temperatures for CO₂ are

synchronized with that for H₂ evolution, which can be interpreted that the reaction between activated carbon stemmed from CH₄ dissociation and the adsorbed oxygen species proceeds. It is further suggested that the adsorbed oxygen species can effectively eliminate the deposition carbon. With the consumption of adsorbed oxygen species, CO formation starts due to the shortage of oxygen resource. Probably, the part of lattice oxygen species also participates in the reaction, leading to forming CO. Besides, in term of CO₂ and CO formation temperature, the catalysts show the following orders of 3NZH < 3NZN < 3NZO, which is confirmed that the 3NZH catalyst possessed the most active adsorbed oxygen species and the highest mobility of lattice oxygen species.

Furthermore, it is worthy to note that CH₄ dissociation and H₂ evolution still take place at above 745 °C (Fig. 7a and b) for the three catalysts, whereas CO₂ and CO are not produced (Fig. 7c and d) during the CH₄-TPSR process. This is considered as the homogeneous thermal decomposition of CH₄ [47].

3.3. Catalytic performance for the DRM

We studied the catalytic activity of the Ni catalysts supported the three ZrO₂ samples in the DRM, all 3 wt % Ni/ZrO₂ catalysts were tested at 700 °C using a GHSV of 24 000 mL/(g·h). As shown in Fig. 8, the test results clearly suggest that the performance of 3NZH catalyst is superior to that of 3NZN and 3NZO catalysts.

From Fig. 8a and b, it is observed that both CH₄ and CO₂ conversions over the 3NZH catalyst are higher than that on 3NZN and 3NZO catalysts during the time on stream (TOS). As mentioned above, the Ni dispersion of the prepared catalysts is so approximate (corresponding to the similar particle size) that its contribution to catalytic performance is not decisive. Simultaneously, the interaction between Ni and ZrO₂, and the morphology and structure of ZrO₂ are almost same. Therefore, for the present catalysts, the difference in their catalytic activity should be mainly related with oxygen species distribution over the catalyst

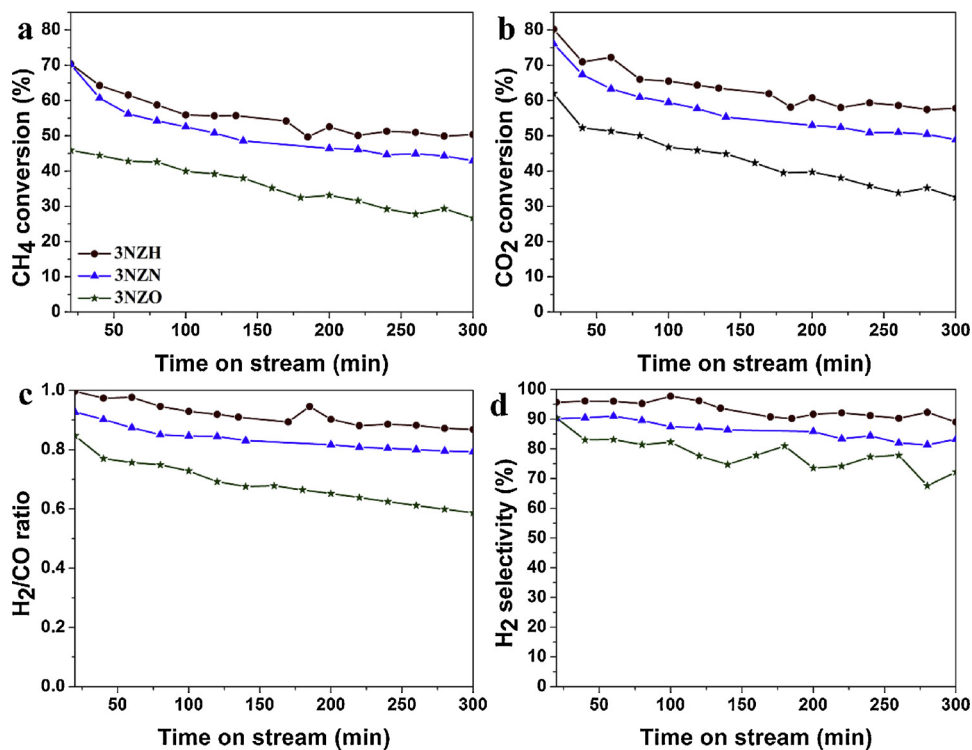


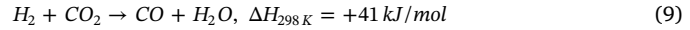
Fig. 8. The performance of Ni-containing catalysts supported by ZrO₂ samples treated under different atmospheres (H₂, N₂ and O₂) for the DRM. Reaction conditions: atmospheric pressure, T = 700 °C, CH₄/CO₂ = 1/1, GHSV = 24 000 mL/(g·h).

surface. Here, it can be suggested that the highest activity over 3NZH catalyst with slightly low Ni dispersion is mainly ascribed to the most adsorbed oxygen species over its surface. Though 3NZN catalyst possesses relatively less adsorbed oxygen species than 3NZH catalyst, these two catalysts show close initial CH₄ conversion, which is probably related to the relatively high Ni dispersion of the former. It is clear that because of its relatively low Ni dispersion and the fewest adsorbed oxygen species, the activity over 3NZO catalyst is the lowest among the three catalysts.

Further, CH₄ and CO₂ conversions over the three catalysts exhibit a decreasing trend during the TOS. But the decrease rate of CH₄ conversion over the 3NZH catalyst (4.0%/h) is much smaller than that over the 3NZN catalyst (7.0%/h). Interestingly, the decrease rate of CH₄ conversion over the 3NZO catalyst (3.8%/h) is the smallest among the three catalysts, which is probably attributed to its lowest activity in the DRM.

Because of the highest ability of CO₂ adsorption and activation (based on the DRIFTS experiments) and CH₄ dissociation over the ZRH samples (based on the TPSR experiments), it is easily understandable that the 3NZH catalyst shows the most excellent performance for the DRM as expected among the three catalysts. Moreover, the adsorbed oxygen species have been well identified to be able to restrain the carbon formation. Therefore, we can conclusively realize that more adsorbed oxygen species over the ZrO₂ surface can promote the performance for Ni/ZrO₂ catalysts in the DRM.

The functions of H₂/CO ratio in the outlet as time on stream are shown in Fig. 8c. It can be observed that H₂/CO ratio for the catalysts shows the following sequence: 3NZH > 3NZN > 3NZO, which indicates that the side-reaction: reversed water gas shift reaction (RWGS, Eq. (9)), is the mildest over the 3NZH catalyst. Moreover, H₂ selectivity in the products, shown in the Fig. 8d, further confirms the results. Thus, the large amounts of adsorbed oxygen species over the catalysts surface not only improve the performance of the catalysts but also drive the H₂/CO ratio near to the theoretical value of 1.0 through restraining the RWGS.



As a clearer notion, the curves of the component proportion in the outlet are shown in Fig. S6. Very obviously, according to the independent curves of CH₄ and CO₂, the component proportions show an increasing trend. It is illustrated that the conversions of CH₄ and CO₂ decrease on the stream. For the curves of CO and H₂ in the product (Fig. S6), although the proportions of both H₂ and CO decrease during the reaction process, the differences between H₂ and CO increase, according with the H₂/CO ratio results (shown in Fig. 8c). This is because the side-reaction RWGS becomes more active as the DRM progress.

Some literatures [48,49] have ever been aware of the correlation between the catalytic behavior and the different surface oxygen species caused by calcining the catalysts under different atmospheres in the DRM. In those researches, higher amount of Ni loading ($\geq 10\%$) was adopted so that the Ni particle size has relatively large differences on different catalysts in the previous system. Moreover, the textural properties (or morphology) of the catalysts employed in their work were also different due to the different calcination atmospheres. Therefore, the reaction behaviors of the catalysts were more or less affected by the change of Ni particle size and the morphology. Thus, their reported results showed that the catalyst with the best performance was not the one treated in H₂ atmosphere, inconsistent with the present result. For this perspective, the previous researches about this theme did not give an intrinsic interpretation for the effects of surface oxygen species on the DRM enough despite that the relation between the amount of adsorbed oxygen species and the performance had been noted. Besides, the analysis of oxygen species in the articles was too simple to support their ideas. Therefore, in our present paper, we have attempted to investigate the effect of single factor (surface oxygen species) on the DRM.

3.4. Characterization of the spent Ni/ZrO₂ catalysts

As demonstrated in many studies [9,15,50], the deactivation of Ni based catalyst is mainly caused by the carbon deposition in the DRM.

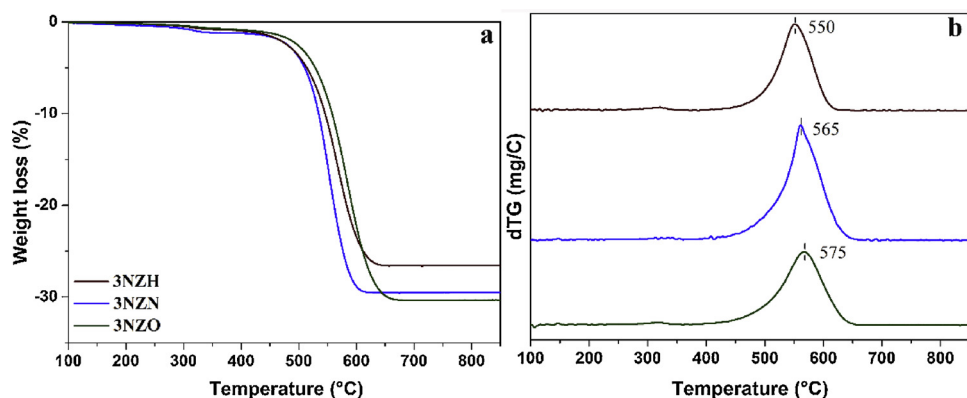


Fig. 9. TG (a) and DTG (b) profiles of the spent Ni-containing catalysts supported by ZrO_2 samples treated under different atmospheres (H_2 , N_2 and O_2).

To quantify the amount of carbon deposited on the spent catalysts surface during the reaction, the TG technique was employed and the profiles are displayed in Fig. 9a. It is figured out that the weight loss of the spent catalysts increases in the following order: 3NZH (26.7%) < 3NZN (29.4%) < 3NZO (30.4%). The 3NZH catalyst possesses the lowest weight loss, suggesting its higher carbon-resistant ability. Thus, it is proved that the higher ratio of adsorbed oxygen species over the catalyst is, the greater the ability of carbon resistance is.

DTG profiles were obtained by taking the 1 st-derivative of thermogravimetric chart. As shown in Fig. 9b, the DTG profiles of the three spent catalysts display only one peak above 550 °C, revealing that only one type of carbonaceous species is eliminated during the TG process. Referring to literatures [4,45], it is known that the deposited carbon species are attributed to the inert carbon with degrees of graphitization, which is mainly responsible for the catalyst deactivation. Since the inert carbon formed is difficultly removed, the catalyst deactivation easily proceeds with the increase of the deposited carbon. Even so, the carbon formation on the catalyst of 3NZH is a bit more active than that of the other two catalysts of 3NZN and 3NZO.

Raman spectra is another reliable technique to analyze the properties of the deposited carbon, mainly the graphitic degree of coke [51]. Fig. 10a presents the Raman spectra of the spent catalysts within the range of 1 200–1 800 cm^{-1} . Two bands, corresponding for the D and G vibration modes of carbon materials, are observed in the Raman spectra. The D band, around 1 340 cm^{-1} , is attributed to disordered-induced Raman scattering from sp^2 carbons, while the G band, which was around 1 570 cm^{-1} , was referred to condensed, ordered or graphitic aromatic structures. As reported [15,52], the intensity ratio between G band and D band (I_G/I_D) represents graphitic degree of carbon deposition. Namely, the higher I_G/I_D reveals the increasing graphitic

degree. From Fig. 10a, the I_G/I_D ratio of 3NZH (1.11) is lower than that of 3NZN (1.15) and 3NZO (1.32), which means that the graphitic degree of the deposited carbon on the surface of 3NZH catalyst is relatively low compared with the other two catalysts. The results accord with the DTG results perfectly.

To further investigate the state of carbonaceous deposition, H_2 -TPH experiments of the spent catalysts were conducted, and the results are shown in Fig. 10b. As observed, there is only one peak of TPH (around 600 °C) for every catalyst, related to the hydrogenation of the inert carbon [53]. After the careful notion, the TPH temperature peak of ZRH catalyst is slightly lower than other two, suggesting the deposited carbon on the 3NZH catalyst surface is a bit more active, in good agreement with the DTG and Raman analysis.

3.5. Discussion

Ni/ZrO_2 catalysts with different oxygen species distribution over the surface have been applied for the DRM to investigate the effects of surface oxygen species on CO_2 adsorption and activation, also included the performance for the DRM. It has been identified that the adsorbed oxygen species over the catalyst surface are favorable for CO_2 adsorption and activation. Besides, they have also been considered to be assistant and responsible for the CH_4 dissociation.

It should be noted that the Ni dispersion is inevitable to possess more or less difference, as shown in this paper, although the texture properties of support are as the same to under control as hoped. However, CH_4 -TPSR result has demonstrated that the Ni dispersion is not a main factor to affecting the catalytic performance over our present prepared catalysts. Thus, not surprisingly, the catalyst with the most adsorbed oxygen species, that is, 3NZH catalyst, is able to display the most excellent performance during the DRM.

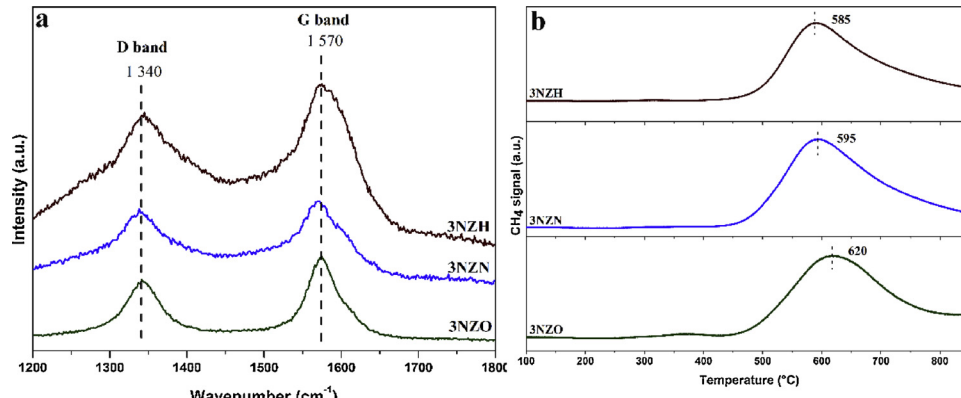


Fig. 10. Raman spectra (a) and H_2 -TPH profiles (b) of the spent Ni-containing catalysts supported by ZrO_2 samples treated under different atmospheres (H_2 , N_2 and O_2).

To further elucidate the influences of the adsorbed oxygen species over the catalyst surface on the performance, the turnover of frequency (TOF) of CH₄ has been derived and listed in **Tab. S3**. According to the above discussed results that the Ni dispersion over 3NZH catalyst is relatively low, the TOF over 3NZH catalyst (2.32 s⁻¹) is the highest among the present three catalysts. This further indicates that the adsorbed oxygen species are of vital importance/indispensability to improve the catalytic performance in the DRM. For comparison, the referred TOF results of CH₄ during the DRM over Ni-based catalyst reported in the recent years are listed in **Tab. S3**. It is observed that core-shell catalyst such as Ni@SiO₂ apparently possesses relatively larger TOF value than the supported catalyst. As aforementioned, Ni particle size on catalyst strongly affects the catalytic performances on the DRM and CH₄ dissociation. Owing to the much smaller size of Ni core (usually < 10 nm) encapsulated by SiO₂ than supported catalyst, the core-shell Ni@SiO₂ catalysts show more preferable advantage in the activity, thereby leading to high TOF value. Moreover, one should bear in mind that the TOF is closely related to the operation parameters such as the feed gas composition, reaction temperature, and GHSV, etc. As also observed, the TOFs of our present catalysts are not the highest, probably is related to the moderate dispersion. However, it needs to be pointed out that the main concern of this paper prefers to investigate the effects of oxygen species over the surface on the DRM to understand the original difference in catalytic performance, which probably provides one major reference to design and develop a catalyst with high activity and stability for the DRM.

On the other hand, as mentioned above, the adsorbed oxygen species are also efficient to remove the deposited carbon to alleviate the catalyst deactivation. Based on the listed results, specifically, the adsorbed oxygen species over 3NZH catalyst have the superexcellent ability to improve the performance for the DRM.

4. Conclusions

ZrO₂ samples, with different oxygen species distribution over the surface, were successfully obtained by treatment under H₂, N₂, and O₂ atmospheres. Moreover, the crystalline structure and textural properties of ZrO₂ samples were identified to possess no obvious difference. The redox ability of the atmosphere strongly affects the distribution of the oxygen species (including the lattice oxygen species and the adsorbed oxygen species). Concretely, the treatment under H₂ flow is able to promote the formation of the most adsorbed oxygen species over the ZrO₂ surface, the following is the treatment under N₂ flow, and the oxidizing atmosphere is the most unfavorable.

In addition, this paper further illustrates that the nickel loading as low as 3 wt% does not cause substantial changes on the support property. It has been also pointed out that there only exist slight differences for the state of Ni particles over different supports, whose contribution to the catalytic performance is not decisive or even negligible. On this basis, it is clearly recognized that the surface oxygen species of ZrO₂ support has great influences on both the CO₂ adsorption and activation and CH₄ dissociation. Specifically, catalyst with higher ratio of adsorbed oxygen to lattice oxygen exhibits more excellent ability to activate CO₂ and CH₄.

Based on the best performance in the DRM over the 3NZH catalyst, it is, here, realized that increasing adsorbed oxygen species over the catalyst surface is really effective to promote the catalytic activity and restrain the side-reaction (RWGS). Simultaneously, the adsorbed oxygen species are effective for suppressing/removing the deposited carbon, thereby alleviating catalyst deactivation.

Acknowledgements

The authors gratefully acknowledge the financial support from the National Natural Science Foundation of China (21303242) and Natural Science Foundation of Shanxi Province (2015011021), China.

Appendix A. Supplementary data

Supplementary material related to this article can be found, in the online version, at doi:<https://doi.org/10.1016/j.apcatb.2018.11.068>.

References

- [1] D. Pakhare, J. Spivey, A review of dry (CO₂) reforming of methane over noble metal catalysts, *Chem. Soc. Rev.* 43 (2014) 7813–7837.
- [2] A.T. Ashcroft, A.K. Cheetham, M.L.H. Green, P.D.F. Vernon, Partial oxidation of methane to synthesis gas using carbon dioxide, *Nature* 352 (1991) 225–226.
- [3] S. Dama, S.R. Ghodke, R. Bobade, H.R. Gurav, S. Chilukuri, Active and durable alkaline earth metal substituted perovskite catalysts for dry reforming of methane, *Appl. Catal. B Environ.* 224 (2018) 146–158.
- [4] J.A. Mendoza-Nieto, S. Tehuacanero-Cuapa, J. Arenas-Alatorre, H. Pfeiffer, Nickel-doped sodium zirconate catalysts for carbon dioxide storage and hydrogen production through dry methane reforming process, *Appl. Catal. B Environ.* 224 (2018) 80–87.
- [5] A. Haryanto, S. Fernando, N. Murali, S. Adhikari, Current status of hydrogen production techniques by steam reforming of ethanol: a review, *Energy Fuel* 19 (2005) 2098–2106.
- [6] B. Christian Enger, R. Lødeng, A. Holmen, A review of catalytic partial oxidation of methane to synthesis gas with emphasis on reaction mechanisms over transition metal catalysts, *Appl. Catal. A Gen.* 346 (2008) 1–27.
- [7] C. Song, W. Pan, Tri-reforming of methane: a novel concept for catalytic production of industrially useful synthesis gas with desired H₂/CO ratios, *Catal. Today* 98 (2004) 463–484.
- [8] L. Pino, C. Italiano, A. Vita, M. Laganà, V. Recupero, Ce_{0.70}La_{0.20}Ni_{0.10}O_{2-δ} catalyst for methane dry reforming: influence of reduction temperature on the catalytic activity and stability, *Appl. Catal. B Environ.* 218 (2017) 779–792.
- [9] Z. Shang, S. Li, L. Li, G. Liu, X. Liang, Highly active and stable alumina supported nickel nanoparticle catalysts for dry reforming of methane, *Appl. Catal. B Environ.* 201 (2017) 302–309.
- [10] V.Y. Bychkov, Y.P. Tyulenin, A.A. Firsova, E.A. Shafranovsky, A.Y. Gorenberg, V.N. Korchak, Carbonization of nickel catalysts and its effect on methane dry reforming, *Appl. Catal. A Gen.* 453 (2013) 71–79.
- [11] J.R. RostrupNielsen, J.H.B. Hansen, CO₂-reforming of methane over transition metals, *J. Catal.* 144 (1993) 38–49.
- [12] D. Baudouin, U. Rodemerck, F. Krumeich, A.D. Mallmann, K.C. Szeto, H. Ménard, L. Veyre, J.P. Candy, P.B. Webb, C. Thieuleux, Particle size effect in the low temperature reforming of methane by carbon dioxide on silica-supported Ni nanoparticles, *J. Catal.* 297 (2013) 27–34.
- [13] J.W. Han, J.S. Park, S.C. Min, H. Lee, Uncoupling the size and support effects of Ni catalysts for dry reforming of methane, *Appl. Catal. B Environ.* 203 (2017) 625–632.
- [14] Z.Y. Hou, P. Chen, H.L. Fang, X.M. Zheng, T. Yashima, Production of synthesis gas via methane reforming with CO₂ on noble metals and small amount of noble-(Rh)-promoted Ni catalysts, *Int. J. Hydrogen Energy* 31 (2006) 555–561.
- [15] R. Rabelo-Neto, H. Sales, C. Inocêncio, E. Varga, A. Oszko, A. Erdohelyi, F. Noronha, L. Mattos, CO₂ reforming of methane over supported LaNiO₃ perovskite-type oxides, *Appl. Catal. B Environ.* 221 (2018) 349–361.
- [16] L. Li, S. He, Y. Song, J. Zhao, W. Ji, C.T. Au, Fine-tunable Ni@porous silica core-shell nanocatalysts: synthesis, characterization, and catalytic properties in partial oxidation of methane to syngas, *J. Catal.* 288 (2012) 54–64.
- [17] Z.W. Li, L.Y. Mo, Y. Kathiraser, S. Kawi, Yolk-satellite-shell structured Ni-yolk@Ni@SiO₂ nanocomposite: superb catalyst toward methane CO₂ reforming reaction, *ACS Catal.* 4 (2014) 1526–1536.
- [18] J.L. Pu, K. Nishikado, N.N. Wang, T.T. Nguyen, T. Maki, E.W. Qian, Core-shell nickel catalysts for the steam reforming of acetic acid, *Appl. Catal. B Environ.* 224 (2018) 69–79.
- [19] J.H. Bitter, K. Seshan, J.A. Lercher, Mono and bifunctional pathways of CO₂/CH₄ reforming over Pt and Rh based catalysts, *J. Catal.* 176 (1998) 93–101.
- [20] D. Pakhare, V. Schwartz, V. Abdelsayed, D. Haynes, D. Shekhawat, J. Poston, J. Spivey, Kinetic and mechanistic study of dry (CO₂) reforming of methane over Rh-substituted La₂Zr₂O₇ pyrochlores, *J. Catal.* 316 (2014) 78–92.
- [21] F. Wang, L. Xu, J. Zhang, Y. Zhao, H. Li, H.X. Li, K. Wu, G.Q. Xu, W. Chen, Tuning the metal-support interaction in catalysts for highly efficient methane dry reforming reaction, *Appl. Catal. B Environ.* 180 (2016) 511–520.
- [22] X. Yu, N. Wang, W. Chu, M. Liu, Carbon dioxide reforming of methane for syngas production over La-promoted NiMgAl catalysts derived from hydrotalcites, *Chem. Eng. J.* 209 (2012) 623–632.
- [23] T. Stroud, T.J. Smith, E. Le Saché, J.L. Santos, M.A. Centeno, H. Arellano-Garcia, J.A. Odriozola, T.R. Reina, Chemical CO₂ recycling via dry and bi reforming of methane using Ni-Sn/Al₂O₃ and Ni-Sn/CeO₂-Al₂O₃ catalysts, *Appl. Catal. B Environ.* 224 (2018) 125–135.
- [24] K. Tanabe, Surface and catalytic properties of ZrO₂, *Mater. Chem. Phys.* 13 (1985) 347–364.
- [25] D. Liu, X.Y. Quek, W.N.E. Cheo, R. Lau, A. Borgna, Y. Yang, MCM-41 supported nickel-based bimetallic catalysts with superior stability during carbon dioxide reforming of methane: effect of strong metal-support interaction, *J. Catal.* 266 (2009) 380–390.
- [26] Y. Lou, M. Steib, Q. Zhang, K. Tiefenbacher, A. Horváth, A. Jentys, Y. Liu, J.A. Lercher, Design of stable Ni/ZrO₂ catalysts for dry reforming of methane, *J. Catal.* 356 (2017) 147–156.

[27] J.W. Hu, V.V. Galvita, H. Poelman, C. Detavernier, G.B. Marin, Catalyst-assisted chemical looping auto-thermal dry reforming: spatial structuring effects on process efficiency, *Appl. Catal. B Environ.* 231 (2018) 123–136.

[28] V.M. Gonzalez-Delacruz, R. Pereniguez, F. Temero, J.P. Holgado, A. Caballero, Modifying the size of nickel metallic particles by H_2/CO treatment in Ni/ZrO₂ methane dry reforming catalysts, *ACS Catal.* 1 (2011) 82–88.

[29] R.K. Singha, A. Shukla, A. Yadav, S. Adak, Z. Iqbal, N. Siddiqui, R. Bal, Energy efficient methane tri-reforming for synthesis gas production over highly coke resistant nanocrystalline Ni-ZrO₂ catalyst, *Appl. Energ.* 178 (2016) 110–125.

[30] X. Zhang, Q. Zhang, N. Tsubaki, Y. Tan, Y. Han, Influence of zirconia phase on the performance of Ni/ZrO₂ for carbon dioxide reforming of methane, *ACS Symp. Ser.* (2015) 135–153.

[31] X. Zhang, Q. Zhang, N. Tsubaki, Y. Tan, Y. Han, Carbon dioxide reforming of methane over Ni nanoparticles incorporated into mesoporous amorphous ZrO₂ matrix, *Fuel* 147 (2015) 243–252.

[32] K.T. Jung, A.T. Bell, The effects of synthesis and pretreatment conditions on the bulk structure and surface properties of zirconia, *J. Mol. Catal. A Chem.* 163 (2000) 27–42.

[33] Y. Zhang, Y. Zhan, C. Chen, Y. Cao, X. Lin, Q. Zheng, Highly efficient Au/ZrO₂ catalysts for low-temperature water-gas shift reaction: effect of pre-calcination temperature of ZrO₂, *Int. J. Hydrogen Energy* 37 (2012) 12292–12300.

[34] R. Srinivasan, B.H. Davis, O.B. Cavin, C.R. Hubbard, Crystallization and phase transformation process in zirconia: an in situ high-temperature X-ray diffraction study, *J. Am. Ceram. Soc.* 75 (1992) 1217–1222.

[35] P. Wongmaneeenil, B. Jongsomjit, P. Praserthdam, Influence of calcination treatment on the activity of tungstated zirconia catalysts towards esterification, *Catal. Commun.* 10 (2009) 1079–1084.

[36] J.F. Moulder, W.F. Stickle, P.E. Sobol, K.D. Bomben, *Handbook of X-ray Photoelectron Spectroscopy*, Perkin-Elmer, Eden Prairie, MN, 1992, p. 52.

[37] M.C. Bradford, M.A. Vannice, CO₂ reforming of CH₄ over supported Pt catalysts, *J. Catal.* 173 (1998) 157–171.

[38] N. Wang, K. Shen, L. Huang, X. Yu, W. Qian, W. Chu, Facile route for synthesizing ordered mesoporous Ni-Ce-Al oxide materials and their catalytic performance for methane dry reforming to hydrogen and syngas, *ACS Catal.* 3 (2013) 1638–1651.

[39] A. Palmqvist, M. Wirde, U. Gelius, M. Muhammed, Surfaces of doped nanophasic cerium oxide catalysts, *Nanostruct. Mater.* 11 (1999) 995–1007.

[40] A. Lofberg, J. Guerrero-Caballero, T. Kane, A. Rubbens, L. Jalowiecki-Duhamel, Ni/CeO₂ based catalysts as oxygen vectors for the chemical looping dry reforming of methane for syngas production, *Appl. Catal. B Environ.* 212 (2017) 159–174.

[41] E.M. Köck, M. Kogler, T. Bielz, B. Klötzter, S. Penner, In situ FT-IR spectroscopic study of CO₂ and CO adsorption on Y₂O₃, ZrO₂, and yttria-stabilized ZrO₂, *J. Phys. Chem. C* 117 (2013) 17666–17673.

[42] Y. Pan, P. Kuai, Y. Liu, Q. Ge, C. Liu, Promotion effects of Ga₂O₃ on CO₂ adsorption and conversion over a SiO₂-supported Ni catalyst, *Energ. Environ. Sci.* 3 (2010) 1322–1325.

[43] S.E. Collins, M.A. Baltanás, A.L. Bonivardi, Infrared spectroscopic study of the carbon dioxide adsorption on the surface of Ga₂O₃ polymorphs, *J. Phys. Chem. B* 110 (2006) 5498–5507.

[44] B. Bachiller-Baeza, I. Rodriguez-Ramos, A. Guerrero-Ruiz, Interaction of carbon dioxide with the surface of zirconia polymorphs, *Langmuir* 14 (1998) 3556–3564.

[45] V. Danghyun, S.C. Novoa, A. Mukasyan, E.E. Wolf, Pressure dilution, a new method to prepare a stable Ni/fumed silica catalyst for the dry reforming of methane, *Appl. Catal. B Environ.* 234 (2018) 178–186.

[46] S. Damyanova, B. Pawelec, R. Palcheva, Y. Karakirova, M.C.C. Sanchez, G. Tyuliev, E. Gaigneaux, J.L.G. Fierro, Structure and surface properties of ceria-modified Ni-based catalysts for hydrogen production, *Appl. Catal. B Environ.* 225 (2018) 340–353.

[47] G. Pantaleo, V.L. Parola, F. Deganello, R.K. Singha, R. Bal, A.M. Venezia, Ni/CeO₂ catalysts for methane partial oxidation: synthesis driven structural and catalytic effects, *Appl. Catal. B Environ.* 189 (2016) 233–241.

[48] J.Q. Zhu, X.X. Peng, L. Yao, X.J. Deng, H.Y. Dong, D.M. Tong, C.W. Hu, Synthesis gas production from CO₂ reforming of methane over Ni-Ce/SiO₂ catalyst: the effect of calcination ambience, *Int. J. Hydrogen Energy* 38 (2013) 117–126.

[49] E. Yang, D.J. Moon, CO₂reforming of methane over Ni²⁺/La₂O₃ catalyst without reduction step: Effect of calcination atmosphere, *Top. Catal.* 60 (2017) 697–705.

[50] Z. Xie, B. Yan, S. Kattel, J.H. Lee, S. Yao, Q. Wu, N. Rui, E. Gomez, Z. Liu, W. Xu, L. Zhang, J.G. Chen, Dry reforming of methane over CeO₂-supported Pt-Co catalysts with enhanced activity, *Appl. Catal. B Environ.* 236 (2018) 280–293.

[51] J. Zhang, F. Li, Coke-resistant Ni@SiO₂ catalyst for dry reforming of methane, *Appl. Catal. B Environ.* 176–177 (2015) 513–521.

[52] X. Li, D. Li, H. Tian, L. Zeng, Z. Zhao, J. Gong, Dry reforming of methane over Ni/La₂O₃ nanorod catalysts with stabilized Ni nanoparticles, *Appl. Catal. B Environ.* 202 (2017) 683–694.

[53] J. Kirchner, J.K. Anolleck, H. Losch, S. Kureti, Methanation of CO₂ on iron based catalysts, *Appl. Catal. B Environ.* 223 (2018) 47–59.